ChemComm

COMMUNICATION

View Article Online
View Journal | View Issue

Cite this: *Chem. Commun.*, 2022, **58**, 12576

Received 13th September 2022,
Accepted 18th October 2022

DOI: 10.1039/d2cc05038b

rsc.li/chemcomm

Optimizing phenyl selenide-based BODIPYs as fluorescent probes for diagnosing cancer and drug-induced liver injury *via* cysteine†

Xiaoyan Lu,‡[a] Nannan Wang,‡[a] Yuanfang Tao,‡[a] Jiamin Wang,*[c] Xin Ji,[b] Jinying Liu,[a] Weili Zhao*[ab] and Jian Zhang*[a]

Herein, by optimizing phenyl selenide-based BODIPYs, BDP-Se-MOS was obtained, which possessed resistance to ROS and could selectively detect Cys. BDP-Se-MOS could not only discriminate between normal and cancer cells, but also image Cys levels in tumor-bearing mice in real time as well as image the fluctuations of Cys levels in an APAP-induced DILI model.

Biothiols, such as cysteine (Cys), glutathione (GSH), and homocysteine (Hcy), are considered to be antioxidants and protectors for free radical scavenging in living organisms due to their unique redox properties and nucleophilicity. In several important physiological processes, three biothiols with similar structures play crucial roles. Studies have shown that abnormal Cys concentrations are closely related to cancer, liver damage, Parkinson's disease, Alzheimer's disease and other acute or chronic diseases.[1–3] However, the abnormal fluctuations of Hcy and GSH levels are also intimately associated with cardiovascular diseases and neurological diseases.[4] Cancer, as a chronic disease, seriously threatens human life.[5] Cys, as a highly expressed small molecule in tumors, can be used as a tumor biomarker.[6] In addition, acute diseases are also the health killers of human beings. Among them, drug-induced liver injury (DILI) is an acute liver disease that can lead to liver failure.[7] It has been reported that oxidative stress is caused by the production of free radicals, such as reactive oxygen species (ROS) and reactive nitrogen species (RNS), during drug metabolism which can cause liver damage,[8] while Cys plays a crucial role in biological redox homeostasis.[9,10] Therefore, the detection of Cys in organisms has become an important means to assess oxidative stress.[9]

Among various detection methods, fluorescence sensors have the advantages of high selectivity, outstanding sensitivity and fast response time,[11] and are suitable for studying the function of thiol biomolecules in living systems.[12,13] At present, researchers have developed many fluorescent probes for the detection of biological thiols.[14] In recent years, our team has constructed a series of fluorescent probes for differential detection and selective detection of Cys, Hcy, and GSH by regulating the substituents on the 1-, 3-, 5-, and 7-positions of BODIPY and using the strong nucleophilicity of thiols to explore the relationship between these thiols and diseases.[15,16] Based on the thiol-induced S_NAr substitution–rearrangement reaction, the fluorescent probe we constructed by introducing a thiophenyl at the *meso* position of BODIPY (**BDP-S**) fits this mechanism to distinguish Cys/Hcy and GSH (Scheme 1A).[15] Subsequently, we employed 1,3,5,7-tetramethyl BODIPY as the fluorophore and arylthiol and aryloxy substituents as recognition groups on the *meso*-BODIPY to construct fluorescent probes (Scheme 1A, **BDP-O, S**). Relying on the steric hindrance of the 1, 7-methyl groups to prevent Hcy and GSH intramolecular rearrangements, these probes could simultaneously and distinctively detect Cys and Hcy/GSH.[16] Among them, the leaving ability of the aryloxy group is slower than that of the arylthio group, which may be caused by the electronic properties of oxygen itself. However, using the arylselenyl group of the same family element as the reactive group, the probe **ASeBDP** realized the differential detection of Cys/Hcy and GSH.[17] In this work, Hcy caused a rearrangement reaction, which may be related to the inadequate steric hindrance at the 1- and 7-positions of the BODIPY dye. However, phenylselenide is also easily oxidized by ROS, and the probe **MPhSe-BDP** was more suitable for detecting HClO.[18]

Herein, we designed and synthesized three fluorescent probes (**BDP-Se-M**, **BDP-Se-MOP** and **BDP-Se-MOS**, Scheme 1B). With increasing degree of substituent conjugation, the selectivity and detection wavelength region of the probes for Cys, Hcy and GSH were significantly different. Based on DFT calculations, the

[a] *Key Laboratory for Special Functional Materials of Ministry of Education, School of Materials Science and Engineering, Henan University, Kaifeng, 475004, P. R. China. E-mail: jianzhang@henu.edu.cn*
[b] *School of Pharmacy, Institutes of Integrative Medicine, Fudan University, Shanghai, 201203, P. R. China. E-mail: zhaoweili@fudan.edu.cn*
[c] *Key Laboratory of Natural Medicine and Immuno-Engineering of Henan Province, Henan University, Kaifeng 475004, China. E-mail: jmwang@henu.edu.cn*

† Electronic supplementary information (ESI) available: Materials and methods, and supporting figures. See DOI: https://doi.org/10.1039/d2cc05038b

‡ These authors contributed equally to this work.

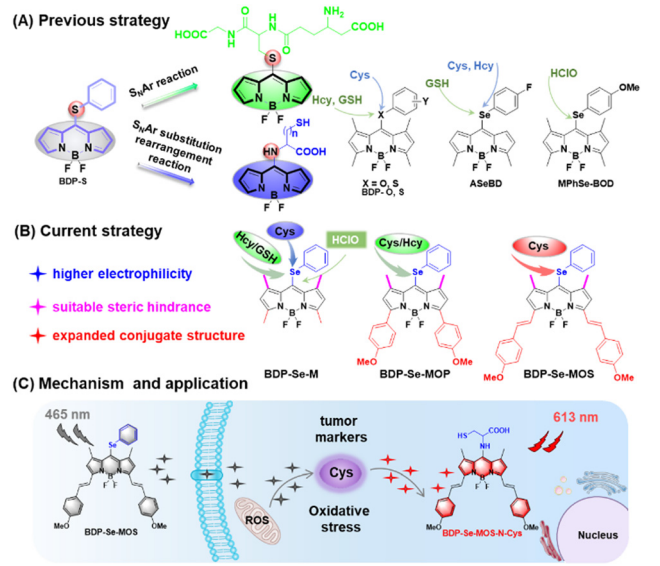

Scheme 1 Design strategies and application prospects of fluorescent probes.

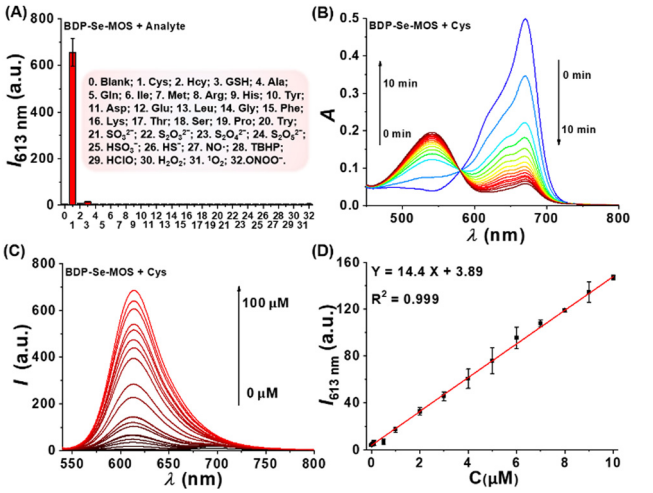

Fig. 1 (A) Fluorescence response of **BDP-Se-MOS** (10 μM) to various analytes (100 μM). λ_{ex} = 525 nm and λ_{em} = 613 nm. (B) The time-dependent absorption spectral changes of **BDP-Se-MOS** (10 μM) with 10 equiv. of Cys. (C) Fluorescence spectra of 10 μM **BDP-Se-MOS** and 0–100 μM Cys. (D) Linear relationship between the fluorescence intensity of **BDP-Se-MOS** and Cys concentration.

excellent antioxidant properties of **BDP-Se-MOS** were speculated to be due to its shortest C–Se bond length and largest C–Se bond order. Mass spectrometry showed that the reaction of **BDP-Se-MOS** with Cys and Hcy/GSH was based on S_NAr substitution/rearrangement induced by different thiol groups. Furthermore, **BDP-Se-MOS** has been successfully applied to monitor endogenous and exogenous Cys in cells, zebrafish and mice. Meanwhile, it could also distinguish normal cells from cancer cells, and realize the imaging of tumor-bearing mouse models. It was also capable of diagnosing APAP-induced DILI in cells and mouse models, and evaluating the repair effect of hepatoprotective drugs such as NAC. The details of all compounds are described in the ESI.†

Firstly, we performed simple selectivity tests on three probes. As shown in Fig. S1 (ESI†), the responses of **BDP-Se-M** to biothiols were similar with previous probes.[16] After adding Cys to the **BDP-Se-M** solution, probe exhibited fluorescence enhancement about 45-fold at 494 nm under excitation at 365 nm. Reacting with Hcy/GSH, 24-fold and 70-fold fluorescence enhancement at 540 nm was captured under excitation at 456 nm. For **BDP-Se-MOP**, only under excitation at 456 nm, Cys/Hcy resulted in approximately 60-fold and 50-fold fluorescence enhancement at 566 nm (Fig. S2, ESI†). For **BDP-Se-MOS**, just addition of Cys could cause significant changes in the absorbance. Under excitation at 525 nm, an approximately 120-fold fluorescence enhancement was obtained at 613 nm (Fig. S3, ESI†). Therefore, **BDP-Se-MOS** was more suitable for selective detection of Cys.

As we considered in the design, phenylselenide was also easily oxidized by ROS, so we performed selectivity experiments with the three probes. The probes were incubated with biologically important amino acids, reactive sulfur species, and reactive nitrogen and oxygen species, respectively. For **BDP-Se-M**, the probe not only responded to Cys/Hcy and GSH, but also showed a significant fluorescence increase upon reacting with ROS, in which HClO caused more than 53-fold fluorescence enhancement (Fig. S4, ESI†). Reassuringly, the fluorescence intensity increased significantly after adding Cys/Hcy to the **BDP-Se-MOP** solution and there was no response to ROS (Fig. S5, ESI†). Meanwhile, **BDP-Se-MOS** with a stronger conjugated structure had a higher fluorescence response only to Cys (Fig. 1A). Notably, the coexistence of interfering analytes did not affect the selective recognition of Cys/Hcy by **BDP-Se-MOP** or Cys by **BDP-Se-MOS** (Fig. S6 and S7, ESI†). Moreover, we investigated the orbital energy levels, C–Se bond lengths and bond orders of the three probes by DFT calculations. The bond lengths and bond orders of C–Se showed that as the conjugation degree of probe increases, the bond lengths decreased and the bond orders increased (Table S1, ESI†). Therefore, **BDP-Se-MOP** and **BDP-Se-MOS** were difficult to be oxidized by ROS. Meanwhile, the energy gap tends to shrink, which was consistent with the sequential redshift of the absorption spectrum of the probe (Fig. S8, ESI†). Therefore, the suitable steric hindrance created by introducing methyl groups at the 1- and 7-positions of BODIPY and the conjugation degree regulated by different *p*-methoxyaryl groups at the 3- and 5-positions could synergistically optimize the response performance of the probes.

Based on the above results, the speculated sensing mechanism of **BDP-Se-MOS** and Cys is shown in Fig. S9 (ESI†). The biothiols attacked the phenylselenide position of the probe for the S_NAr reaction. Only Cys induced intramolecular cyclization rearrangement to form the amino-substituted derivative **BDP-Se-MOS-N-Cys**. Mass spectrometry of **BDP-Se-MOS** was performed in the presence of biothiols (Cys and Hcy) (Fig. S10, ESI†). The results were consistent with the mechanism speculated.

We further investigated the time-dependent responses of **BDP-Se-MOP** and **BDP-Se-MOS** to the biothiols. After adding Cys to the **BDP-Se-MOS** solution, the maximum absorption peak at 675 nm decreased rapidly and the new absorption peak

at 545 nm gradually increased (Fig. 1B). Correspondingly, the fluorescence intensity at 613 nm rapidly increased and completely responded within 10 min (Fig. S11, ESI†). In contrast, when **BDP-Se-MOP** reacted with Cys/Hcy, the absorption peak blue-shifted, and the fluorescence intensity gradually increased, reaching equilibrium in 2 min and 45 min, respectively (Fig. S12, ESI†).

Next, we investigated the fluorescence titration experiments of the two probes. For **BDP-Se-MOS**, the absorption showed a clear blueshift with increasing Cys concentration (Fig. S13, ESI†). Meanwhile, the fluorescence intensity gradually increased at 613 nm and showed a good linear relationship with 0–10 μM Cys (Fig. 1C and 1D). The limit of detection (LOD) was estimated to be 33 nM. As shown in Fig. S14 (ESI†), with the increasing Cys/Hcy concentration, the absorption of **BDP-Se-MOP** showed obvious blueshift, and its fluorescence intensity increased. Moreover, the LODs of **BDP-Se-MOP** for Cys (0–40 μM)/Hcy (0–5 μM) were calculated to be 110 nM and 122 nM, respectively (Fig. S15, ESI†). In addition, the effects of pH on **BDP-Se-MOS** and **BDP-Se-MOP** were also evaluated (Fig. S16 and S17, ESI†). Significantly, **BDP-Se-MOS** could quickly and sensitively monitor the concentration changes of Cys, which is very beneficial for tracking Cys in living systems.

Encouraged by the excellent optical properties of **BDP-Se-MOS**, we explored whether the probe could sensitively and efficiently detect and image Cys in live cells. MTT assay results showed that **BDP-Se-MOS** had good biocompatibility (Fig. S18, ESI†). When HepG2 cells were incubated with **BDP-Se-MOS**, obvious red fluorescence could be observed in the cells. Attenuated fluorescence was observed in cells pretreated with N-ethylmaleimide (NEM, a scavenger of biothiols), but the fluorescence could be lit after the addition of Cys (Fig. S19, ESI†). Since **BDP-Se-MOS** could sensitively detect intracellular Cys, we further explored whether the probe could distinguish normal cells from cancer cells by monitoring the difference in Cys levels. As expected, cancer cells (HepG2 and SMMC-7721) incubated with **BDP-Se-MOS** had a stronger red fluorescence signal than normal cells (QSG-7701 and RAW264.7) (Fig. 2). The difference in fluorescence intensity between cancer cells and normal cells should be due to the difference in intracellular Cys levels.

Based on this, we further evaluated the ability of **BDP-Se-MOS** to recognize and image Cys *in vivo*. As shown in Fig. S20 and S21 (ESI†), **BDP-Se-MOS** could recognize endogenous or exogenous

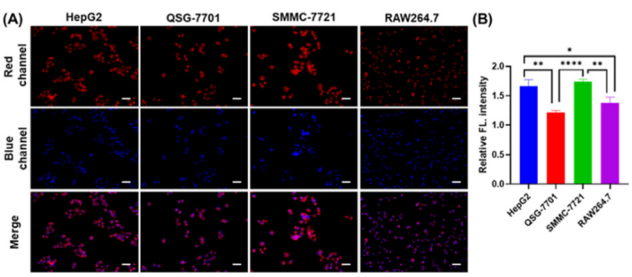

Fig. 2 (A) The fluorescence imaging of cancer cells and normal cells. (B) Fluorescence intensities of (A). ****$P < 0.0001$, **$P < 0.01$, *$P < 0.1$. Scale bar: 50 μm.

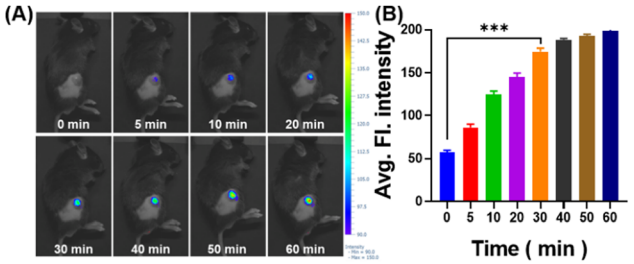

Fig. 3 (A) Fluorescence imaging of tumor mice after injection with **BDP-Se-MOS** at different times. (B) Fluorescence intensities of (A). ***$P < 0.001$. λ_{ex} = 540–580 nm, λ_{em} = 590–670 nm.

Cys in zebrafish and mice. In addition, the fluorescence intensity rapidly increased within 30 min after subcutaneous injection of **BDP-Se-MOS** into the mice, and the fluorescence intensity remained stable within 1 h due to the good photostability of the probe (Fig. S22, ESI†). These experimental results all demonstrated that **BDP-Se-MOS** could be used for sensitive detection and real-time imaging of Cys *in vivo*. According to the literature reported, the concentration of Cys was also overexpressed in tumors.[2,6] As shown in Fig. 3, the fluorescence was enhanced gradually by injecting **BDP-Se-MOS** intratumorally. At 10 min, an obvious fluorescence signal could be observed, which approached the maximum value at 30 min, and it could still be observed after 1 h. Moreover, from bioimaging *via* tail vein injection, obvious fluorescence in the tumor was observed 6 h after injection (Fig. S23, ESI†). All the above results indicated that **BDP-Se-MOS** could realize the detection and imaging of Cys in normal mice and in tumor-bearing mice.

In order to verify the critical role of Cys in DILI, we used probe **BDP-Se-MOS** to explore the changes of Cys levels in an APAP-induced acute liver injury model. As shown in Fig. S24 (ESI†), after pretreatment of cells with APAP, the fluorescence signal was significantly attenuated. Prior to this, an increase in the fluorescence signal was observed when cells were treated with N-acetaminophen (NAC, a hepatoprotective drug). These all should be closely related to oxidative stress during cell damage.

In order to further explore the potential application of **BDP-Se-MOS** *in vivo*, we evaluated the probe to achieve fluorescence imaging of Cys in an APAP-induced liver injury mouse model. The distribution and clearance behaviors of **BDP-Se-MOS** were investigated firstly *via* fluorescence imaging assays. After tail vein injection of the probe at a dose of 1 mg kg^{-1}, the major organs of mice were dissected and imaged at different times (Fig. S25, ESI†). We found that the probe was mainly enriched in the liver of mice, followed by the kidney (Fig. S25A, ESI†). Meanwhile, the corresponding fluorescence intensity values are listed in Fig. S25B (ESI†), which indicated that the maximum fluorescence intensity occurred around 6 h and gradually cleared within 48 h. Then, as expected, distinct fluorescent signals were observed in the livers of normal mice when injecting **BDP-Se-MOS** (Fig. 4A). In contrast, no obvious fluorescent signals were observed in each organ of the mice injected with PBS, which indicated that the fluorescent signals

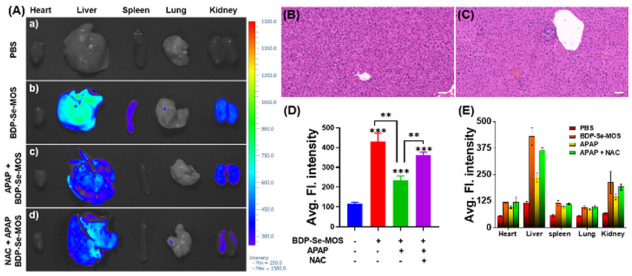

Fig. 4 (A) Fluorescence images of organs from APAP-induced mice. Representative H&E staining of the liver slices from (B) healthy mice and (C) DILI mice. (D) Fluorescence intensities of the liver from A. (E) Fluorescence intensities of A. $^{**}P < 0.01$, $^{***}P < 0.001$. λ_{ex} = 540–580 nm, λ_{em} = 590–670 nm.

of the mouse organs were generated by the reaction between **BDP-Se-MOS** and Cys. We observed weaker fluorescence signals in the liver of the APAP-induced liver injury mouse model. In contrast, the fluorescence intensity in the liver of liver-damaged mice that were administered NAC in advance was significantly increased. These changes in fluorescence intensity were statistically significant (Fig. 4D). Liver injury was also verified in mouse tissue sections (Fig. 4B and C). We observed that the fluorescence signals were mainly concentrated in the liver of the mice, followed by the kidney (Fig. 4E). The above results suggested that **BDP-Se-MOS** could monitor the fluctuations of Cys levels in the APAP-induced mouse model of acute liver injury. Therefore, our probe **BDP-Se-MOS** may provide a new avenue for the diagnosis of acute liver injury.

In summary, by expanding the conjugated structure and regulating the reactivity of the probes, we designed and synthesized three fluorescent probes for biothiols. By optimizing the structure, **BDP-Se-MOS** could selectively detect Cys in the red emission region and possess resistance to ROS. The optimization of the reactivity of the probes was rationalized by DFT calculations. Importantly, **BDP-Se-MOS** had low cytotoxicity and could image endo/exogenous Cys in live cells, zebrafish and mice. It could not only distinguish normal cells and cancer cells, but also monitor Cys levels in tumor-bearing mice in real time. More than that, **BDP-Se-MOS** could also trace the fluctuation of Cys levels in an APAP-induced DILI model. These findings will greatly advance the understanding of the role of Cys in chronic diseases such as cancer and acute liver injury such as DILI.

Xiaoyan Lu: investigation, writing – original draft. Nannan Wang: investigation, writing – original draft. Yuanfang Tao: investigation, compound synthesis, solution testing. Jiamin Wang: conceptualization, writing – review & editing, funding acquisition. Xin Ji: investigation, formal analysis. Jinying Liu: supervision, formal analysis. Weili Zhao: supervision, funding acquisition. Jian Zhang: conceptualization, writing – review & editing, funding acquisition, project administration.

This research was financially supported by the National Natural Science Foundation of China (No. 82030107 and 21702046) and the Key Scientific Research Program of the Higher Education Institution of Henan Province (No. 22A150005). The authors thank Prof. Changwei Gong, School of Materials Science and Technology, Taiyuan University of Science and Technology, for his helpful discussions on the density functional theory calculations.

Conflicts of interest

The authors declare no conflicts of interest.

Notes and references

1 S. Shahrokhian, *Anal. Chem.*, 2001, **73**, 5972–5978.
2 J. Liu, Z.-Q. Wang, G.-J. Mao, W.-L. Jiang, M. Tan, F. Xu and C.-Y. Li, *Anal. Chim. Acta*, 2021, **1171**, 338655.
3 G. Yin, Y. Gan, H. Jiang, T. Yu, M. Liu, Y. Zhang, H. Li, P. Yin and S. Yao, *Anal. Chem.*, 2021, **93**, 9878–9886.
4 (*a*) N. Kwon, C. S. Lim, G. Ko, J. Ha, D. Lee, J. Yin, H. M. Kim and J. Yoon, *Anal. Chem.*, 2021, **93**, 11612–11616; (*b*) S. Seshadri, A. Beiser, J. Selhub, P. F. Jacques, I. H. Rosenberg, R. B. D'agostino, P. W. F. Wilson and P. A. Wolf, *N. Engl. J. Med.*, 2002, **346**, 476–483.
5 F. Bray, J. Ferlay, I. Soerjomataram, R. L. Siegel, L. A. Torre and A. Jemal, *Ca-Cancer J. Clin.*, 2018, **68**, 394–424.
6 Y. Yue, T. Zhao, K. Ma, F. Huo and C. Yin, *Chem. Commun.*, 2022, **58**, 2311–2314.
7 L. Yuan and N. Kaplowitz, *Clin. Liver Dis.*, 2013, **17**, 507–518.
8 (*a*) S. Russmann, G. A. Kullak-Ublick and I. Grattagliano, *Curr. Med. Chem.*, 2009, **16**, 3041–3053; (*b*) G. Fan, N. Wang, J. Zhang, X. Ji, S. Qin, Y. Tao and W. Zhao, *Dyes Pigm.*, 2022, **199**, 110073.
9 C.-X. Yin, K.-M. Xiong, F.-J. Huo, J. C. Salamanca and R. M. Strongin, *Angew. Chem., Int. Ed.*, 2017, **56**, 13188–13198.
10 L. Yue, H. Huang, W. Song and W. Lin, *Chem. Eng. J.*, 2022, **441**, 135981.
11 X. Lu, H. Su, J. Zhang, N. Wang, H. Wang, J. Liu and W. Zhao, *Spectrochim. Acta, Part A*, 2022, **267**, 120620.
12 (*a*) L.-Y. Niu, Y.-S. Guan, Y.-Z. Chen, L.-Z. Wu, C.-H. Tung and Q.-Z. Yang, *J. Am. Chem. Soc.*, 2012, **134**, 18928–18931; (*b*) J. Zhang, N. Wang, X. Ji, Y. Tao, J. Wang and W. Zhao, *Chem. – Eur. J.*, 2020, **26**, 4172–4192.
13 X. Yang, X. Lu, J. Wang, Z. Zhang, X. Du, J. Zhang and J. Wang, *J. Agric. Food Chem.*, 2022, **70**, 3047–3055.
14 (*a*) G. Yin, T. Niu, Y. Gan, T. Yu, P. Yin, H. Chen, Y. Zhang, H. Li and S. Yao, *Angew. Chem., Int. Ed.*, 2018, **57**, 4991–4994; (*b*) J. Yin, Y. Kwon, D. Kim, D. Lee, G. Kim, Y. Hu, J.-H. Ryu and J. Yoon, *J. Am. Chem. Soc.*, 2014, **136**, 5351–5358; (*c*) L.-Y. Niu, Y.-Z. Chen, H.-R. Zheng, L.-Z. Wu, C.-H. Tung and Q.-Z. Yang, *Chem. Soc. Rev.*, 2015, **44**, 6143–6160; (*d*) G. Yin, T. Niu, T. Yu, Y. Gan, X. Sun, P. Yin, H. Chen, Y. Zhang, H. Li and S. Yao, *Angew. Chem., Int. Ed.*, 2019, **58**, 4557–4561.
15 Y. Zhang, X. Shao, Y. Wang, F. Pan, R. Kang, F. Peng, Z. Huang, W. Zhang and W. Zhao, *Chem. Commun.*, 2015, **51**, 4245–4248.
16 J. Zhang, X. Ji, H. Ren, J. Zhou, Z. Chen, X. Dong and W. Zhao, *Sens. Actuators, B*, 2018, **260**, 861–869.
17 Y. Mei, H. Li, C.-Z. Song, X.-G. Chen and Q.-H. Song, *Chem. Commun.*, 2021, **57**, 10198–10201.
18 B. Wang, P. Li, F. Yu, P. Song, X. Sun, S. Yang, Z. Lou and K. Han, *Chem. Commun.*, 2013, **49**, 1014–1016.